UNIVERSITÉ DE GENÈVE

UNIVERSITÉ DE GENÈVE
FACULTÉ DE MÉDECINE

Section de *médecine Clinique*
Département de Radiologie et informatique médicale

Deep learning-assisted artifact reduction in clinical oncological whole-body PET/CT imaging

Mémoire de Master

Directeur de mémoire : Prof. Habib Zaidi

Agathe Pezzoni

31/05/2023

Acknowledgments:
Prof. Habib Zaidi
Isaac Shiri
Yazdan Salimi
Dr Hossein Arabi
Dre Ismini Mainta
Dre Elsa Hervier

Possible conflicts of interest: None

Description of contributions:
The development of the algorithm was conducted by Isaac Shiri and Yazdan Salimi.
The analysis of the 200 images using Osirix and the data entry into Excel were performed by Dre Ismini Mainta and Dre Elsa Hervier from HUG.
The generation of figures and statistical tables were carried out by Shayan Mostafaei from KTH.
For my part, I analyzed 200 cases with Osirix, then, selected with arbitrarily chosen criteria (described in the following article) about 50 interesting cases to analyze. Then I segmented 14 cases including 21 lesions, and finally I wrote this article under the supervision of Isaac Shiri and Prof. Habib Zaidi.
Additionally, Dre Ismini Mainta provided training in Osirix analysis and guided the segmentation process, contributing to my learning and development.
I received in the beginning and throughout the 1,5 years of this work many explanations from Dr Hossein Arabi and Isaac Shiri on the operation of PET/CT and deep learning technology.
And finally, Prof. Habib Zaidi guided me through all the steps of this project.

I. Abstract

Nuclear imaging is becoming increasingly popular in the medical field, particularly for the assessment and staging of cancer. It has become an indispensable tool for healthcare professionals dedicated to delivering optimal patient care. Among nuclear imaging modalities, PET/CT is widely used in the clinic but inherently bears a number of limitations and challenges. This includes the frequent occurrence of artifacts that can results in misdiagnosis or cause significant errors in image interpretation and analysis, mainly during the fusion of PET and CT images. Despite the implementation of protocols aimed at minimizing these artifacts, there are still imperfections. Indeed, the scientific literature has only a few articles dealing with this topic, thus showing a lack of in-depth research in this field. The purpose of this study is to test, in the context of clinical oncology, a new methodology that corrects these artifacts using Artificial Intelligence (AI), in particular Deep Learning (DL) algorithms. The algorithm of this work was developed and described in the article by Shiri et al. (1). After comparing PET/CT and PET-DL images using different metrics, such as image quality, the presence of artifacts, and diagnostic confidence, PET-DL images were found to be significantly superior to conventional PET/CT images.

II. Introduction

Various forms of nuclear imaging, including Positron Emission Tomography (PET) and Single-Photon Emission Tomography (SPECT), are employed for diagnosing various diseases. PET imaging operates by administering a radioactive tracer, for instance ^{18}F-fluorodeoxyglucose (^{18}F-FDG), into the patient's body one hour prior to data acquisition in clinical oncology (2). The interpretation of diagnostic images generated by this imaging modality is challenging primarily due to its poor resolution (e.g. Figure 1a), particularly in critical structures such as the lungs, digestive system, and limbs (indicated by red arrows). In addition, the images suffer from several physical degrading factors, including Compton scattering. This phenomenon is caused by the interaction of annihilation photons with tissues, prior to reaching PET detectors. However, PET imaging offers functional information by revealing characteristics of body’s structures avid to the injected tracer. To compensate for the lack of resolution, PET is combined with Computed Tomography (CT) to provide the anatomical information for mapping (Figure 1b) (3). Besides, the CT scan is used to correct attenuation and scatter caused by the interaction of photons with biological tissues (2). Finally, a fused PET/CT image is formed and is more easily interpretable by nuclear medicine physicians and radiologists (Figure 1c). However, artifacts from CT might translate to the corresponding PET images, and additional artifacts can arise from both PET and CT imaging; the red arrows depicted in Figure 1c highlight the motion and halo artifacts, described below.

One of the well-known artifacts is a mismatch between PET and CT images owing to patient’s breathing, i.e. the motion artifact. Indeed, obtaining PET/CT imaging begins with the acquisition of CT in just a few seconds, followed by PET which takes few minutes (2-3 mins)

per bed position (2), where the patient is breathing normally. This motion artifact leads to diagnostic errors, especially at the thorax/abdomen interface; lesions on the upper part of the liver could appear on the lower part of the right lung and vice versa.

The halo artifact is also manifested by a strong uninterpretable signal on the periphery of areas with a high radiotracer uptake (3). For example, the bladder or kidneys are areas with high tracer uptake on PET, and scatter correction might fail during PET image reconstruction, resulting in a photopenic area near these high uptake regions (4).

The truncation artifact occurs in patients whose body diameter exceeds 50 cm corresponding to the CT scanner's field-of-view (FOV) (5), hence missing the CT image information for PET image correction.

The metallic artifacts are caused by the presence of a metal hip prosthesis or any metallic object within the patient's body. The metal will absorb a large portion of x-ray photons during CT scanning, causing hyperdense streaks to appear on CT images, thus distorting PET attenuation correction by the CT at the level of these streaks, which is particularly problematic for the analysis of possible neighboring lesions (5).

Finally, after describing some artifacts observed in PET/CT imaging, it is worth highlighting that protocols were devised to circumvent them, especially motion artifacts. First, the establishment of a breathing pattern, e.g. tidal breathing described by Blodgett et al. (6) "instructing the patient to breathe with shallow tidal respiration until the detector is near the bottom of the thorax, at which time the patient is instructed to stop breathing wherever they are in their respiratory cycle until the detector has passed through the liver". Second, adding to PET/CT, the assessment of initial PET images prior to CT-based attenuation and scatter correction (PET-nonASC) (7) is recommended to get rid of motion artifacts. Third, respiratory motion tracking by "observing in a noninvasive way, the patient from outside the body" to "obtain motion-free PET and CT images as well as truly spatially coregistered PET and CT data, thus improving both image quality and quantitative accuracy" (8). This is not an exhaustive list of existing solutions, but it does demonstrate the need to correct them in order to avoid diagnostic errors at best.

Indeed, if we compile all nuclear medicine exams referred to the Department of Nuclear Medicine & Molecular Imaging of Geneva University Hospitals (HUG) between 2021 and 2022, 60.3% of the indications were oncology, 33.6% cardiology, and 6.0% neurology. Oncological PET scans, therefore, represent most examinations interpreted by nuclear medicine physicians in this department. According to the study by Pan et al. (9) which analyzed 100 PET/CT images looking for a shift at the diaphragm level caused by breathing, 34% presented this artifact. This finding underscores the significant relevance of this issue within the field of nuclear medicine.

Overall, the reconstruction of PET images with CT-based attenuation and scatter correction is the source of these artifacts. Therefore, novel artificial intelligence (AI) assisted techniques have been developed. Indeed, McMillan and Bradshaw (10) reported that “The ability of AI-based approaches to obviate the need for an additional CT or transmission image greatly improves the capability of existing equipment”. Likewise, Arabi et al. (11) highlighted that “The DLAC [Deep learning-based joint PET attenuation and scatter correction] approach exhibited a very good and consistent performance regardless of the radiotracer used”. The feasibility of a similar approach, referred to as “Deep-JASC” developed by Shiri et al. (12) was demonstrated, concluding that “The proposed algorithm does not require the use of anatomical images (CT or MRI), thus providing a sensible solution in a clinical setting for standalone PET scanners and PET/MRI systems”.

Therefore, this work aimed to demonstrate the necessity to avoid the artifacts of traditional PET/CT and introduce AI as a solution to this problem, with a particular focus on motion artifacts.

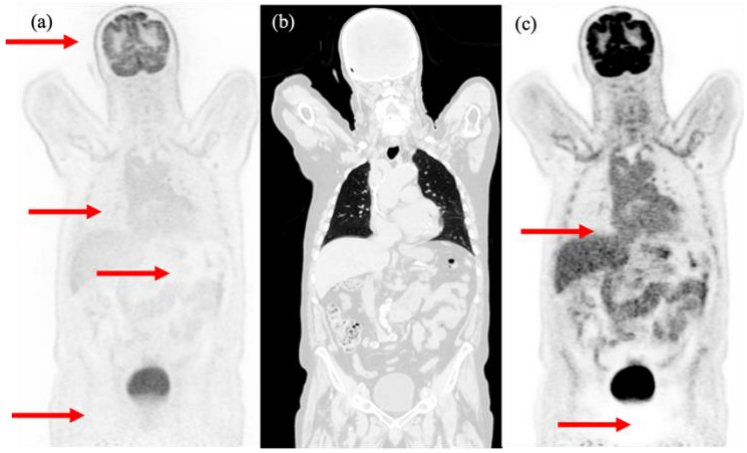

Figure 1. Example of a representative clinical study showing the PET image (a), CT (b), and fused PET/CT images (c). The observed motion and halo artefacts are indicated by the red arrows in the upper and lower parts, respectively.

III. Materials and Methods

1. Patient demographics

This work is based on a retrospective study approved by the Ethics Commission (CCER ID: 2017-00922), involving the recruitment of 2087 patients between May 2017 and September 2022. These were oncology patients who underwent ^{18}F-FDG PET/CT whole-body examinations. This database has been finely sorted to gather the good quality and artifact-free images, 869 in total, to train the AI algorithm and compare them to images with artifacts. The remaining images were therefore placed in the batch of images with artifacts. Next, 100 patients' images with artifacts were randomly selected, forming a set of 200 images including two variants for each image: the first one was corrected for attenuation and scatter using CT (PET-ASC), whereas the second one was corrected using the deep learning-based approach (PET-DL).

2. Qualitative analysis

Two nuclear medicine physicians interpreted blindly the images on Osirix viewer. This batch of 200 images were assessed by filling an Excel file consisting of 6 columns separating the different parts of the body (head/neck, thorax, thorax/abdomen interface, abdomen, pelvis, and limbs). For each part of the body, they had to score the quality of images (excellent, high, medium, poor, very poor), the presence of artifacts (absent, minor, medium, major, unacceptable), diagnostic confidence (excellent, high, medium, poor, very poor) and the number of observed lesions (0-10 and above with the letter M for multiples). Next, 50 images were selected with the following criteria: the presence of a motion artifact at the thorax/abdomen interface, classified at least by "medium" and a minimum of one lesion in this area. Subsequently, in order to eliminate duplicates (same images corrected by CT and DL), the PET-ASC cases were correlated with their PET-DL counterparts using an Excel table that displayed all equivalents. Ultimately, after this image matching, 14 patients with a total of 21 lesions remained in this specific region of interest (thorax/abdomen interface).

3. Quantitative analysis

Twenty-one identified lesions were then segmented using the ITK-SNAP software. To do so, it is necessary to open the CT, PET-ASC, the uncorrected PET image (PET-nonASC), and the PET-DL image simultaneously. Then, the segmentation begins with the selection, in the four images, of voxels plus a margin (the peripheral gray area, which is by definition neither healthy nor pathological) when scrolling up and down the section of the transverse plane. This segmentation can then be coordinated with the other planes. Following the segmentation of lesions, it is possible to extract image-derived metrics, such as the Standardized Uptake Value (SUV), which serves as the unit of measurement used for the quantitative analysis of PET images. This is the standardized way of calculating tracer uptake at a voxel level in malignant lesions (12). Different variants of the SUV metric can be calculated, including the average SUV (SUV_{mean}), which is widely used, the SUV of the most intense voxel within the lesion (SUV_{max}), or the average SUV within a $1cm^3$ region (SUV_{peak}).

The same analysis was carried out on the artifact-free group of images to establish a reference point for interpretation. Bland-Altman analysis was performed to compare the results.

IV. Results

1. Qualitative analysis

The qualitative analysis is based on the direct examination of images and the diagrams containing the information from the Excel files filled by the two nuclear medicine physicians during the analysis of the 200 images.

The red arrows in Figure 2 shows a large shift in the position of the diaphragm between the CT and the PET-nonASC, reflected on the corresponding PET/CT (red square) by a blurred area corresponding to both the lung and the liver. In addition, the difference map, with the red color representing negative bias and the blue the positive bias, highlights this discrepancy. Therefore, the red area at the thorax/abdomen interface corresponds to underestimation of tracer uptake on the PET-ASC compared to the PET-DL. In addition, in Figure 3, the right diaphragmatic dome appears lower on the PET-ASC (red arrow) than on the PET-DL (red arrow).

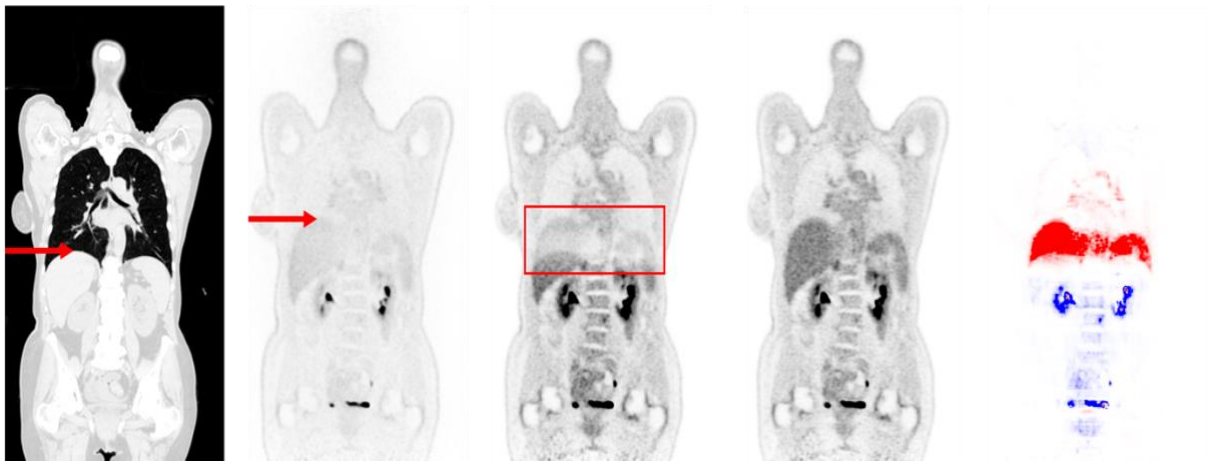

Figure 2. Motion artifact in the diaphragmatic region indicated by the red arrows and red square. From left to right, CT, PET-nonASC, PET-ASC, PET-DL, and difference map (PET-ASC minus PET-DL).

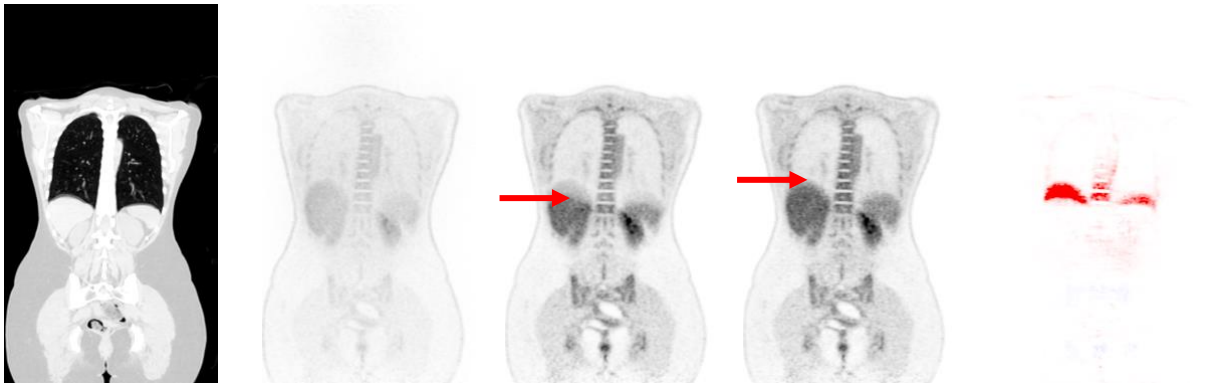

Figure 3. Motion artifact in the diaphragmatic region indicated by the red arrows. From left to right, CT, PET-nonASC, PET-ASC, PET-DL, and difference map (PET-ASC minus PET-DL).

Two cases containing lesions at the thorax/abdomen interface are shown in Figures 4 and 5. In the PET-ASC image, the lesions appear to be in the right lower part of the lung (red arrow), while in the PET-nonASC and PET-DL images, the same lesions are located in the upper part of the liver (red arrows).

Figure 6 illustrates another difference between PET/CT and PET-DL. At the periphery of the bladder, we can see on the PET-ASC image tracer uptake, absent on the PET-DL image. The difference map emphasizes this difference more clearly, with the red color indicating a gap in this region of PET-ASC compared to PET-DL.

Figures 7-9 depict bar charts summarizing the results of the assessment performed by the two nuclear medicine physicians. The assessment of artifacts, image quality, and diagnostic confidence at the "thorax/abdomen interface". First, Figure 7 compares the occurrence of artifacts between PET-ASC and PET-DL with 0.3% of PET-ASC images that do not contain artifacts versus 31.9% for PET-DL images and 39.6% of PET-ASC images presenting with moderate artifacts versus 15.4% for PET-DL images. Second, Figure 8 illustrates image quality assessment of PET-ASC and PET-DL images: 0.5% of PET-ASC images were judged to be of excellent quality compared to 5.5% of PET-DL images. 22.0% of PET-ASC images were classified to be of "high quality" compared to 44.5% of PET-DL images and finally 13.2% of PET-ASC images were rated as poor quality compared to 0.5% for PET-DL. Lastly, Figure 9 compares the diagnostic confidence between these two modalities and indicates that 2.2% of PET-ASC images were classified as presenting "excellent diagnostic confidence" against 4.9% for PET-DL, 50.5% of PET-ASC images classified with "high confidence" against 70.3% in PET-DL and finally 7.1% of PET-ASC images were listed in the category "poor diagnostic confidence" against 4.4% of PET-DL images.

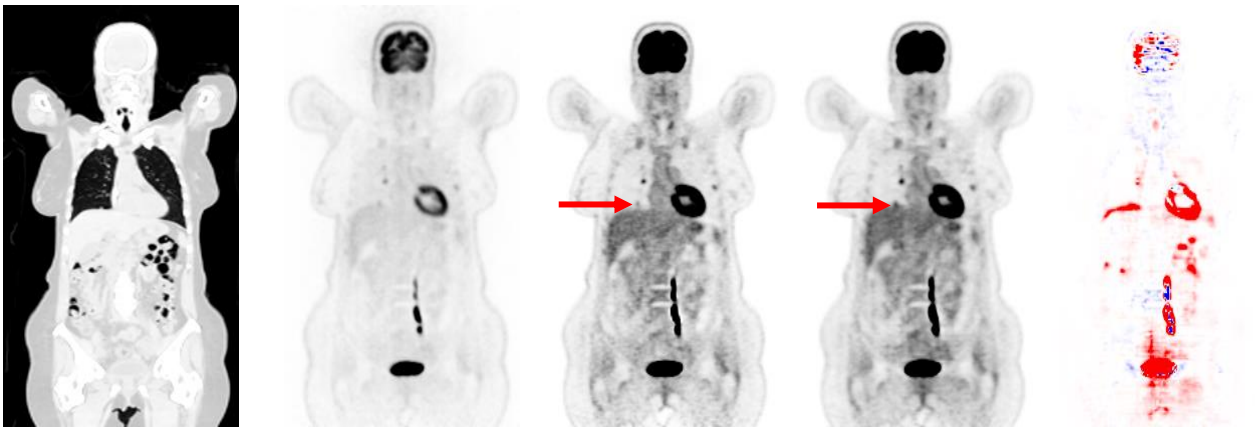

Figure 4. Motion artifact with one hepatic lesion in the diaphragmatic region, indicated by the red arrows. From left to right, CT, PET-nonASC, PET-ASC, PET-DL, difference map (PET-ASC minus PET-DL).

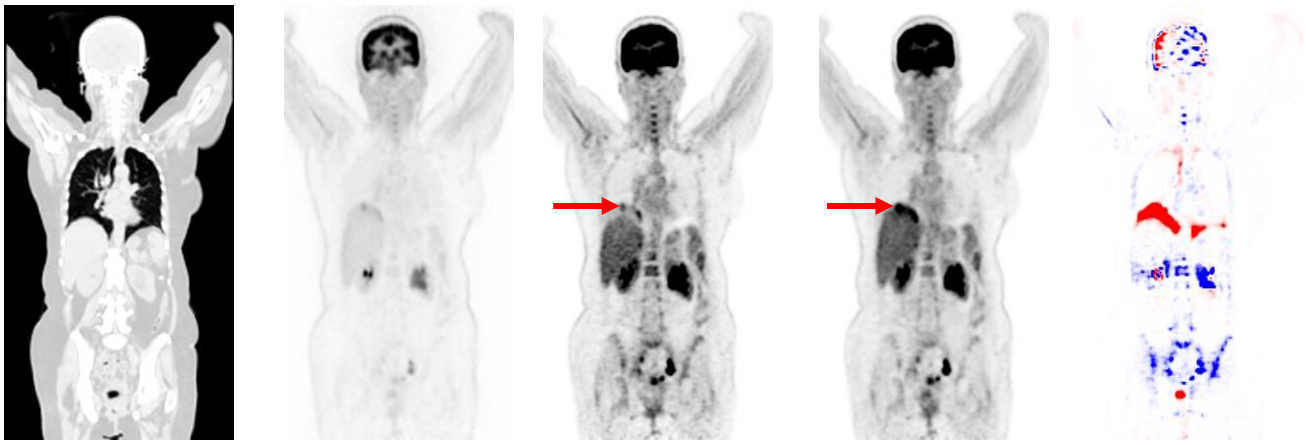

Figure 5. Motion artifact with two hepatic lesions in the diaphragmatic region, indicated by the red arrows. From left to right, CT, PET-nonASC, PET-ASC, PET-DL, difference map (PET-ASC minus PET-DL).

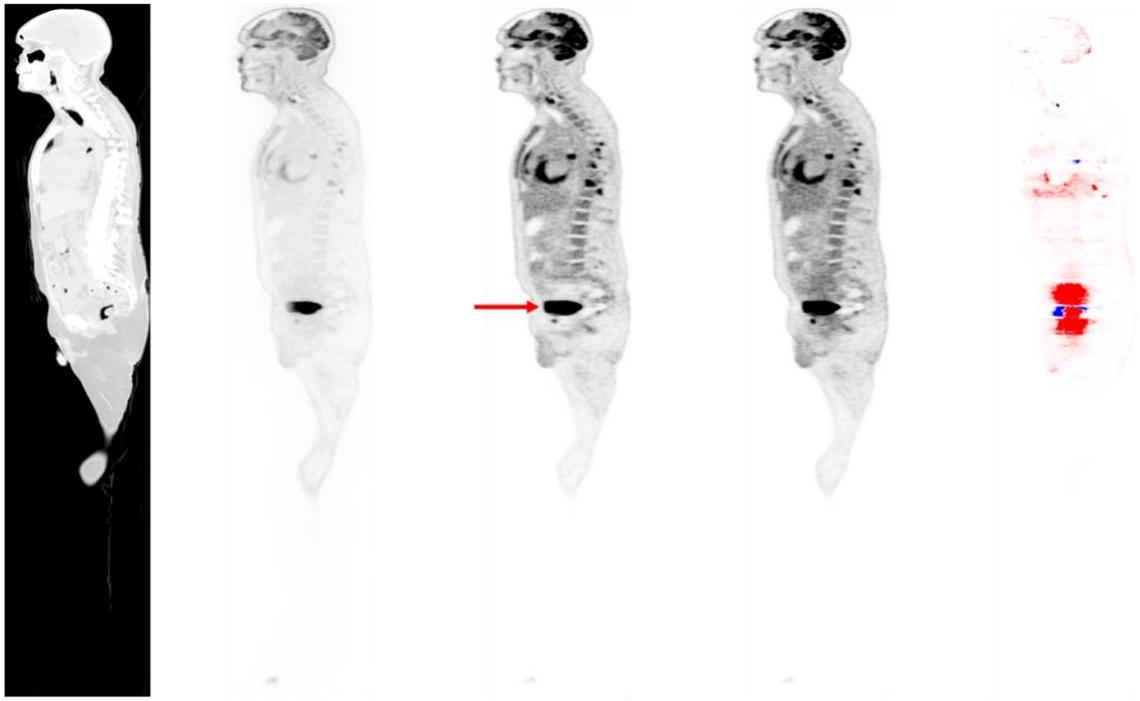

Figure 6. Halo artifact around the bladder indicated by the red arrow. From left to right, CT, PET-nonASC, PET-ASC, PET-DL, difference map (PET-ASC minus PET-DL).

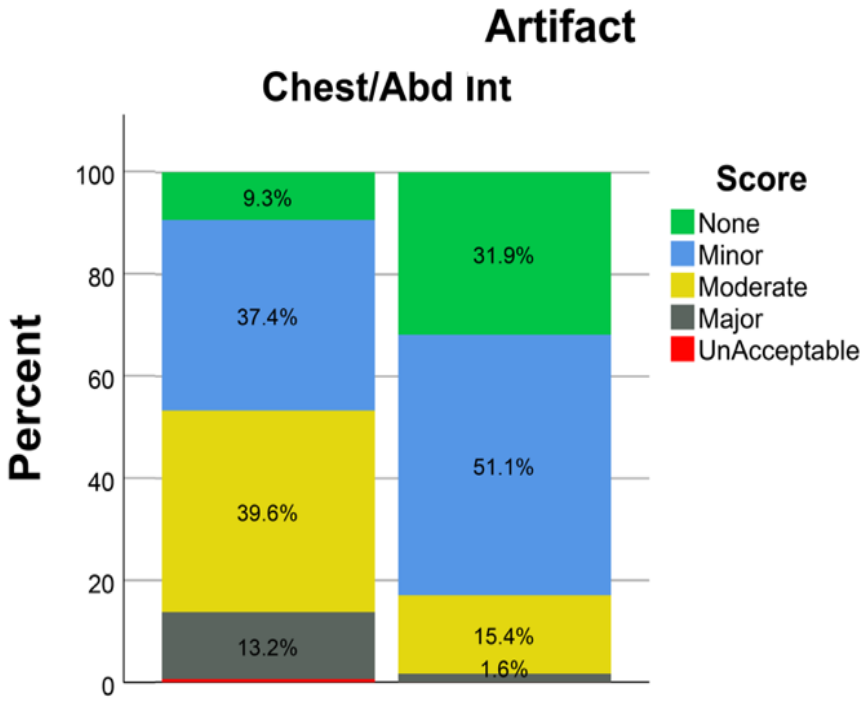

Figure 7. Bar charts comparing the two physicians' appreciation of PET-ASC (left) and PET-DL (right) artifacts.

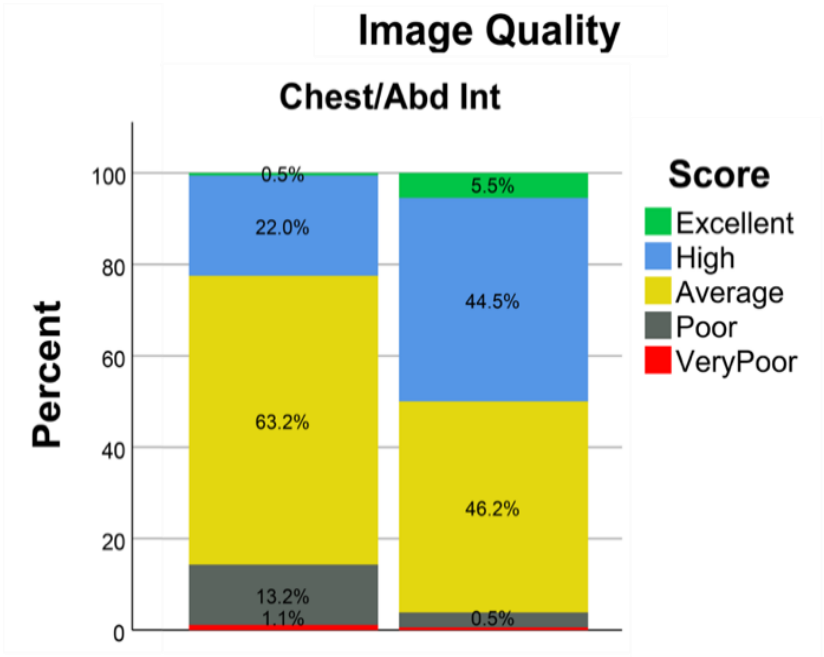

Figure 8. Bar charts comparing the two physicians' assessment of image quality of PET-ASC (left) and PET-DL (right).

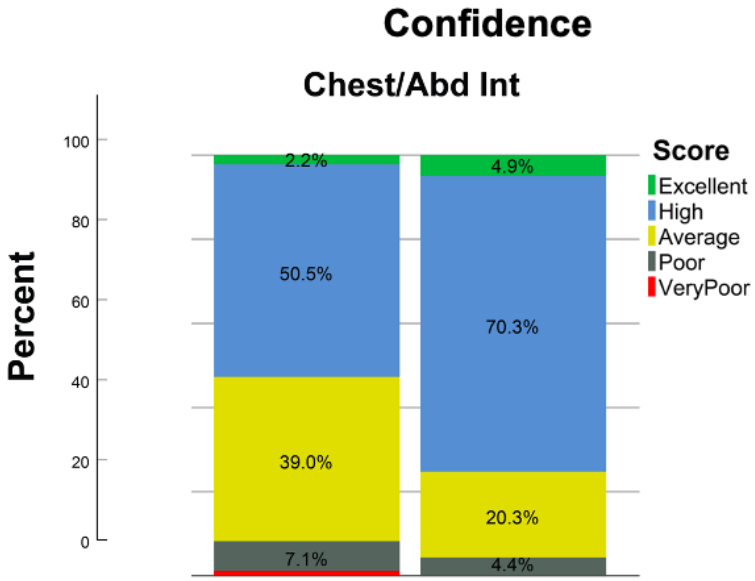

Figure 9. Bar charts comparing the two physicians' appreciation of confidence in diagnosing PET-ASC (left) and PET-DL (right).

2. Quantitative analysis

The Bland-Altman graph shown in Figure 10 shows the quantitative information extracted from the 21 segmented lesions in the 14 patients' images that presented lesions and motion artifacts in the diaphragmatic region. The three charts present the results of SUV_{mean}, $SUV_{max,}$ and SUV_{peak} for the 21 segmented lesions. On the abscissa, the SUV_{mean} of the lesion is plotted whereas the ordinate displays the difference between SUV_{mean}, SUV_{max} et SUV_{peak} of PET-ASC and PET-DL (example of an equation for the first graph: [SUV_{mean} PET-ASC] - [SUV_{mean} PET-DL]).

The difference mean in these three graphics is negative, -1.05±0.70 for SUV_{mean}, -1.77±1.22 for $SUV_{max,}$ and -1.50±1.00 for SUV_{peak} (Figure 10). These results are statistically significant, as demonstrated by a p-value <0.05 (Table 1). However, the differences between PET/CT and PET-DL calculated in the artifact-free image are close to 0, that is 0.02±0.36, 0±0.7, 0.02±0.6, respectively (Figure 11).

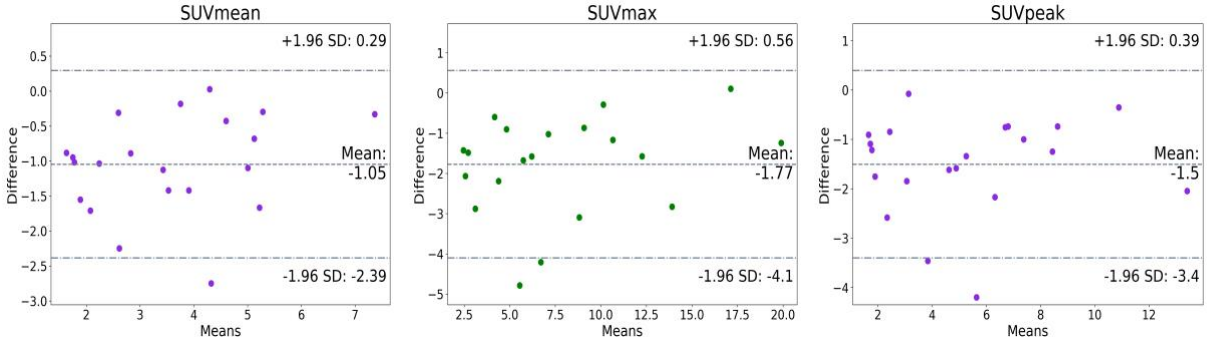

Figure 10. Bland-Altman plots comparing SUV_{mean}, $SUV_{max,}$ and SUV_{peak} of PET-ASC and PET-DL in the set of 14 images.

SUV	Mean	95% CI	Mean	95% CI	P-value
SUVmean	-1.05±0.70	-1.37 to -0.73	1.05±0.70	0.73 to 1.37	0.0001
SUVmax	-1.77±1.22	-2.33 to -1.22	1.78±1.22	1.24 to 2.34	0.0001
SUVpeak	-1.50±1.00	-2.00 to -1.05	1.50±1.00	1.10 to 1.11	0.0001

Table 1. P-values' resulting from the comparison of SUV_{mean}, SUV_{max}, and SUV_{peak} in the set of 14 images.

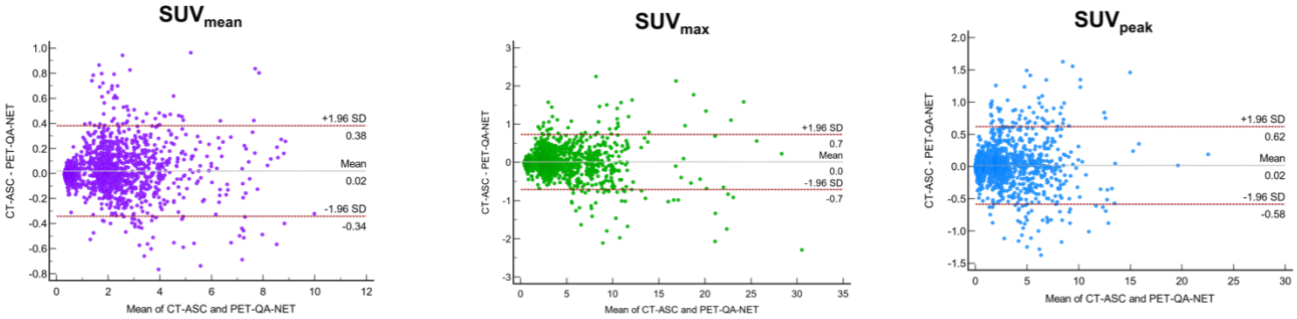

Figure 11. Bland-Altman plots comparing SUV_{mean}, SUV_{max}, and SUV_{peak} of PET-ASC and PET-DL of the artifact-free image set.

V. Discussion

Through the qualitative and quantitative analysis of the 200 images with artifacts and the batch of images from the 14 selected patients, this study revealed the inferiority of PET/CT compared to PET-DL.

The shift in the diaphragm position observed in PET-ASC images in Figures 2 and 3 highlights the potential risk of misdiagnosis, especially if a lesion is present. This risk is further supported by the example shown in Figure 4, where a lesion located on the diaphragmatic side of the liver appears in the lower right lung on the PET-ASC image. However, upon examining the PET-nonASC image, it becomes clear that the lesion is hepatic and not pulmonary. Hence, PET-ASC images may lead to misinterpretation.

This issue is also illustrated in Figure 5, where the motion artifact observed in PET-ASC is absent in PET-DL. This mismatch is also absent in Figures 2 and 3, where liver lesions are

clearly visible in the hepatic level. In addition, the halo artifact visible on PET-ASC in Figure 6 is absent in PET-DL allowing us to analyze the region around the bladder more effectively.

If we compare PET/CT and PET-DL more concretely with the help of the bar charts shown in Figures 7-9, PET-DL is superior to PET/CT in all aspects. PET-DL images are reported as having less artifact, presenting with better image quality and the two nuclear medicine physicians had more diagnostic confidence with PET-DL images than PET/CT.

Regarding quantitative analysis, the negative mean of the differences in SUV_{mean}, SUV_{max} and SUV_{peak} between PET-ASC and PET-DL indicates an underestimation of SUV by PET-ASC (Figure 10). This is the objectivation of the motion artifact because, in images without artifacts, the mean of the difference is zero (Figure 11) since the voxels in this region in PET-ASC and PET-DL have the same SUV (knowing that breathing did not cause a shift on PET/CT). This underestimation of SUV in PET-ASC is clearly visible in Figure 3. The red arrow on PET-ASC image shows a region with a different uptake than in PET-DL image.

The motion and halo artifacts shown in the figures and the other artifacts mentioned in the introduction, such as truncation or metal artifacts, add defects to the PET/CT image. The challenge is that the number of images possessing these artifacts and the extent to which they prevent proper interpretation is difficult to predict. Thank to Shiri et al. (1) and this work, PET-DL images revealed their superiority by removing these barriers to PET image interpretation.

From a more general point of view, the use of AI in medical imaging is growing on different fronts and application fields, including artifacts reduction. A number of studies have been conducted showing strength in the recognition and correction of artifacts caused by CT-based attenuation correction, in particular the one by Shiri et al. (3) which has “constructed and validated a highly effective and fast quality assurance tool that could be used to routinely detect and correct for a number of artifacts, including mismatches and motion, truncation, metal and halo artifacts in PET images”. In addition, the study by Whiteley et al. (13) presented a methodology for PET image reconstruction using AI: “The results showed that the proposed neural network produced images nearly equivalent to using the full count data and superior to conventional reconstruction of the same data”. Besides, a study specifically addressing metal artifacts by Gjesteby et al. (14) reported that “deep learning can be a viable tool to address CT reconstruction challenges”.

Finally, the objective is not to replace CT with AI but rather to utilize AI as an additional imaging tool for further evaluation. While adding another CT scan is sometimes necessary due to artifacts, AI can eliminate the need for this step, leading to faster processing, cost reduction, and minimizing radiation exposure (10).

VI. Conclusion

The clinical application of a deep learning algorithm for PET attenuation and scatter correction has demonstrated notable advantages, including a significant reduction in image artifacts, improved image quality increased diagnostic confidence. In addition, the use of AI in this context offers more benefits, such as radiation dose reduction to the patient. Overall, this method is well suited to complement and improve the interpretation of PET/CT images.

VII. References

1. Shiri I, Salimi Y, Hervier E, Pezzoni A, Sanaat A, Mostafaei S, et al. Artificial Intelligence-Driven Single-Shot PET Image Artifact Detection and Disentanglement: Towards Routine Clinical Image Quality Assurance. Eur J Cancer *submitted*
2. Ratib O. Revue Médicale Suisse : Le scanner PET-CT : nouvel outil d'imagerie moléculaire. Rev Médicale Suisse. 2004;62(2490):1470–4.
3. Shiri I, Sanaat A, Salimi Y, Akhavanallaf A, Arabi H, Rahmim A, et al. PET-QA-Net: Towards Routine PET Image Artifact Detection and Correction using Deep Convolutional Neural Networks. In: 2021 IEEE Nuclear Science Symposium and Medical Imaging Conference (NSS/MIC) [Internet]. Piscataway, NJ, USA: IEEE; 2021 [cited 2023 Feb 17]. p. 1–3. Available from: https://ieeexplore.ieee.org/document/9875610/
4. Heußer T, Mann P, Rank CM, Schäfer M, Dimitrakopoulou-Strauss A, Schlemmer HP, et al. Investigation of the halo-artifact in 68Ga-PSMA-11-PET/MRI. PLOS ONE. 2017 Aug 17;12(8):e0183329.
5. Bockisch A, Beyer T, Antoch G, Freudenberg L, Kuhl H, Debatin J, et al. Positron emission tomography/computed tomography?imaging protocols, artifacts, and pitfalls. Mol Imaging Biol. 2004 Aug;6(4):188–99.
6. Blodgett TM, Mehta AS, Mehta AS, Laymon CM, Carney J, Townsend DW. PET/CT artifacts. Clin Imaging. 2011 Jan;35(1):49–63.
7. Truong MT, Viswanathan C, Carter BW, Mawlawi O, Marom EM. PET/CT in the Thorax: Pitfalls. Radiol Clin North Am. 2014 Jan 1;52(1):17–25.
8. Bettinardi V, De Bernardi E, Presotto L, Gilardi MC. Motion-Tracking Hardware and Advanced Applications in PET and PET/CT. PET Clin. 2013 Jan;8(1):11–28.
9. Pan T, Mawlawi O, Nehmeh SA, Erdi YE, Luo D, Liu HH, et al. Attenuation correction of PET images with respiration-averaged CT images in PET/CT. J Nucl Med Off Publ Soc Nucl Med. 2005 Sep;46(9):1481–7.
10. McMillan AB, Bradshaw TJ. Artificial Intelligence–Based Data Corrections for Attenuation and Scatter in Position Emission Tomography and Single-Photon Emission Computed Tomography. PET Clin. 2021 Oct;16(4):543–52.
11. Arabi H, Bortolin K, Ginovart N, Garibotto V, Zaidi H. Deep learning-guided joint attenuation and scatter correction in multitracer neuroimaging studies. Hum Brain Mapp. 2020 Sep;41(13):3667–79.
12. Shiri I, Arabi H, Geramifar P, Hajianfar G, Ghafarian P, Rahmim A, et al. Deep-JASC: joint attenuation and scatter correction in whole-body 18F-FDG PET using a deep residual network. Eur J Nucl Med Mol Imaging. 2020 Oct 1;47(11):2533–48.
13. Whiteley W, Luk WK, Gregor J. DirectPET: full-size neural network PET reconstruction from sinogram data. J Med Imaging. 2020 May;7(3):032503.
14. Gjesteby L, Yang Q, Xi Y, Zhou Y, Zhang J, Wang G. Deep learning methods to guide CT image reconstruction and reduce metal artifacts. In: Medical Imaging 2017: Physics of Medical Imaging [Internet]. SPIE; 2017 [cited 2023 Apr 4]. p. 752–8. Available from: https://www.spiedigitallibrary.org/conference-proceedings-of-spie/10132/101322W/Deep-learning-methods-to-guide-CT-image-reconstruction-and-reduce/10.1117/12.2254091.full